ACS APPLIED MATERIALS & INTERFACES

Research Article

www.acsami.org

One-Step Preparation and Assembly of Aqueous Colloidal CdS_xSe_{1-x} Nanocrystals within Mesoporous TiO_2 Films for Quantum Dot-Sensitized Solar Cells

Xiaohui Song, Minqiang Wang,* Jianping Deng, Zhi Yang, Chenxin Ran, Xiangyu Zhang, and Xi Yao

Electronic Materials Research Laboratory (EMRL), Key Laboratory of Education Ministry; International Center for Dielectric Research, Xi'an Jiaotong University, Xi'an, 710049, China

Supporting Information

ABSTRACT: In the field of quantum dots (QDs)-sensitized solar cells, semiconductor QDs sensitizer with a moderate band gap is required in order to sufficiently match the solar spectrum and achieve efficient charge separation. At present, changing the size of QDs is the main method used for adjusting their band gap through quantum size effect, however, the pore sizes of mesoporous TiO_2 film set a limit on the allowed size of QDs. Therefore, the tuning of electronic and optical properties by changing the particle size could be limited under some circumstances. In this paper, high-quality aqueous CdS_xSe_{1-x} QDs sensitizer is successfully synthesized and effectively deposited on a mesoporous TiO_2 film by a one-step hydrothermal method. In addition to size, alloy QDs provide composition as an additional dimension for tailoring their electronic properties. The alloy composition and band gap can be precisely controlled by tuning the precursor ($Se/Na_2S{\cdot}9H_2O$) ratio while maintaining the similar particle size. By using such CdS_xSe_{1-x} sensitized TiO_2 films as photoanodes for solar cell, a maximum power conversion efficiency of 2.23% is achieved under one sun illumination (AM 1.5 G, 100 mW cm^{-2}).

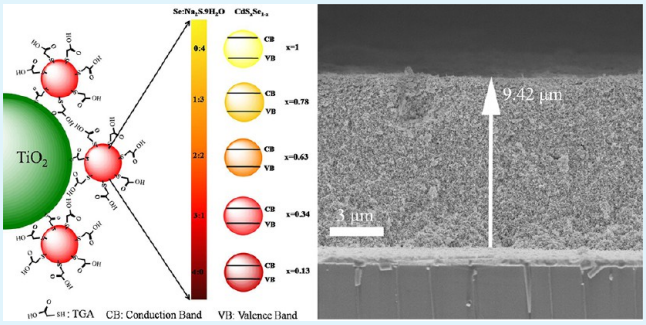

KEYWORDS: *quantum dots-sensitized solar cells, hydrothermal reaction, compositional tuning, cadmium sulfide selenide, titanium dioxide*

1. INTRODUCTION

Semiconductor nanocrystals (NCs), often referred to as quantum dots (QDs), have attracted considerable interest for the development of solar cell devices because of their fascinating optoelectronic properties. The band gap of QDs can be tuned by controlling their size, and therefore, their absorption spectra can be tailored to match the solar spectrum;[1,2] they have a higher extinction coefficient than conventional dyes,[3] large intrinsic dipole moment favoring charge separation.[4,5] Moreover, the QDs open up a way to utilize hot electrons and to generate multiple electron−hole pairs with a single photon through impact ionization.[6−8] For these reasons, solar cells based on QDs may have the potential to exceed the Schockley-Queisser limiting efficiency. A typical strategy to construct solar cells based on QDs is to use semiconductor QDs as light absorber to sensitize wide-band gap metal oxide (TiO_2, ZnO, SnO_2) nanostructure films.[9−13] In recent years, a lot of work on QDs-sensitized solar cells (QDSSC) has been reported where sensitization was achieved using binary CdS,[9,10] CdSe,[14,15] or PbS QDs, and in some cases cosensitization using more than one of these materials.[16−18] However, up until to now, the cell performance reported on QDSSC has still been much lower than that of conventional dye-sensitized solar cells, and the reported best power conversion for liquid junction QDSSCs are typically below 7%.[18−20]

One of the current key issues in increasing QDSSC efficiency is to search for suitable panchromatic sensitizers to enhance the harvest of solar light. As reported in numerous publications over the past few years, tuning the size of QDs is the major way of adjusting the band gap energy to widen their absorption range.[14,17,18] However, among those binary QDs sensitizers, the tuning span of optical absorption by the size-dependent quantum confinement effect is relatively narrow in the visible light range.[21] For example, the absorbent peak of CdS QDs was adjusted between 330 and 480 nm,[22,23] whereas that of CdSe QDs was tunable from 500 to 640 nm.[24,25] In addition, to be embedded into pores of mesoporous TiO_2 films, QDs have to be engineered with proper sizes to be compatible with those of the pores. On the other hand, in order to inject the excited electrons from QDs sensitizer to TiO_2, a type-II band alignment between them is highly desired, where both the conduction and valence bands of QDs should be higher in energy than that of TiO_2. Therefore, it is important for one QD

Received: March 18, 2013
Accepted: May 9, 2013
Published: May 9, 2013

   dx.doi.org/10.1021/am4009924 | ACS Appl. Mater. Interfaces 2013, 5, 5139−5148

ensemble to satisfy the requirement of both size and band gap energy, from an application point of view. It has thus become a challenge to be able to tune the optical properties of QDs independent of their size. One solution to the above problems is to employ alloyed QDs as sensitizer. Since the physical and optical properties of alloyed QDs depend on both size and composition, it is possible to tune the band gap by altering component stoichiometric ratios in alloyed QDs even at a constant size. Thus, by varying composition, we gain a second tool for tuning the optical and electronic properties of QDs. Employing composition-tunable alloyed QDs as sensitizer will enable us to take advantage of quantum confinement effects to improve the optical absorption process without overly impeding the subsequent transport of charge to TiO_2 electrodes.[26] For example, solar cells containing PbSe QDs have been found to exhibit large short-circuit photocurrent densities (J_{SC}), while those with PbS QDs have shown large open-circuit voltages (V_{OC}).[27] With the construction of photovoltaic cells containing PbS_xSe_{1-x} alloy QDs, an enhancement in both J_{SC} and V_{OC} was realized, resulting in higher power conversion efficiency relative to those of the constituent binary systems.[28] Therefore, alloyed QDs provide an alternative approach in selecting desirable properties for the construction of high-performance QDSSC.

Among II−VI group colloidal QDs, CdSe and CdS QDs are most intensively investigated.[9−11] At room temperature, the lattice constants of zinc-blende CdSe and CdS are 6.050 and 5.835 Å, respectively.[29] Owing to the small lattice mismatch, CdS and CdSe are miscible over a wide range of compositions, which leads to the formation of CdS_xSe_{1-x} ($0 \le x \le 1$) alloy QDs with almost zero enthalpy change.[17] CdS_xSe_{1-x} alloy QDs have significant importance in photonics and electronics, since it has a direct and widely modulated band gap from 1.73 to 2.44 eV corresponding to the composition change from CdSe to CdS. CdS_xSe_{1-x} QDs could therefore be used as an efficient sensitizer for TiO_2.

To date, much work has been committing to the preparation of CdS_xSe_{1-x} ternary alloyed QDs, and the optical and electrical properties have also been investigated,[30−32] but the use of CdS_xSe_{1-x} as sensitizer in QDSSC has seldom been reported in the literature.[17,33,34] In the present study, a series of CdS_xSe_{1-x} QD-sensitized mesoporous TiO_2 films with controlled composition and light harvesting were synthesized using a relatively simple and facile approach, viz. the in situ hydrothermal method. In this method, the composition and band gap of the obtained alloyed CdS_xSe_{1-x} QDs can be easily controlled by changing the $Se/Na_2S{\cdot}9H_2O$ feed molar ratio, and thus the absorption spectrum of the CdS_xSe_{1-x} sensitized TiO_2 films can be easily tuned in the range of 506−662 nm while maintaining the similar particle size. Using these alloyed CdS_xSe_{1-x} QD-sensitized TiO_2 (TiO_2/CdS_xSe_{1-x}) films as photoanodes for QDSSC, a maximum power conversion efficiency of 2.23% was achieved under simulated AM1.5 100 mW cm^{-2} illumination.

2. EXPERIMENTAL SECTION

2.1. Preparation of Mesoporous TiO_2 Films. Prior to the fabrication of TiO_2 films, FTO glass plates (Pilkington TEC 15, sheet resistance: 15 Ω sq^{-1}) were cleaned in a detergent solution using an ultrasonic bath for 30 min and rinsed with water and ethanol. Mesoporous TiO_2 films were prepared by screen printing of a TiO_2 slurry (homemade P25 paste) on the FTO glass, and the printed films were then sintered in air by heating gradually to 325 °C and holding for 5 min, then 375 °C for 5 min, at 450 °C for 15 min, and finally at 500 °C for 15 min. The projected area of the TiO_2 films was 0.5 × 0.5 cm^2. The thickness of the sintered TiO_2 films was approximately 10 μm measured by a profilometer Dektack 6 from Veeco.

2.2. Deposition of CdS_xSe_{1-x} QDs on TiO_2 Films. CdS_xSe_{1-x} precursor solution was prepared by the addition of freshly prepared oxygen-free aqueous Se and S source mixture into the Cd precursor reaction medium. Cd precursor solutions were prepared by mixing 1.25 mmol of $Cd(CH_3COO)_2$ and stabilizer of TGA in 25 mL of deionized water under vigorous stirring. The solution was first turbid because of the poor solubility of the Cd-TGA complex, which was dissolved by raising the pH to 11.5 with 5 M NaOH solution. Oxygen-free KHSe solution was prepared by mixing appropriate amount of Se powders into 10 mL of aqueous KBH_4 solution. The Se:KBH_4 mole ratio of 1:3 was maintained in this experiment. After complete reduction of Se, appropriate amount of $Na_2S{\cdot}9H_2O$ was added to the KHSe solution. The total concentration of Se and Na_2S was fixed at 0.12 mmol and the molar ratios of Se to $Na_2S{\cdot}9H_2O$ were varied from 0:4, 1:3, 2:2, and 3:1 to 4:0. Then, 1 mL of the above mixture was added to the prepared Cd precursor solutions. Finally, the resultant solution was transferred into a Teflon-lined stainless autoclave with a volume of 40 mL, and before that a screen-printed TiO_2 film was already put into the autoclave. The sealed autoclave was put into an oven and maintained at 160 °C for 12 h to promote the growth and assembly of CdS_xSe_{1-x} QDs on TiO_2. Afterward, the autoclave was cooled to room temperature by a hydro-cooling process, and the TiO_2 films were taken out and washed with distilled water to remove excess reactants, followed by drying in a N_2 flow.

2.3. Assembly of the QDSSCs. The thus prepared TiO_2/CdS_xSe_{1-x} photoanode was placed on the Pt-sputtered conducting glass electrode (ITO/Pt) to fabricate the full cell. The two electrodes were separated by a piece of 45 μm thick Surlyn film and sealed up by heating. The internal space was filled with polysulfide electrolyte of 1 M Na_2S, 1 M S, and 0.1 M NaOH in methanol/water (4:6 by volume). The hole made on the counter electrode glass for injecting electrolyte was sealed by a Surlyn film and microscope cover glass. Three cells were prepared at each condition to ensure the credibility of the research results, and the experimental results showed that the variation of efficiency was lower than 11% (see the Supporting Information, S1), which suggested that this hydrothermal method has good reproducibility.

2.4. Characterization. The morphology of the bare TiO_2 and TiO_2/CdS_xSe_{1-x} photoanodes were characterized by using a Hitachi S-4800 field-emission scanning electron microscope (FESEM) equipped with an X-ray energy dispersive spectrometer (EDX). Transmission electron micrographs (TEM) were recorded by a JEOL-2010F high-resolution transmission electron microscope (HRTEM). The phase compositions and crystal structures of the as-synthesized photoanodes and CdS_xSe_{1-x} QDs were determined by X-ray powder diffraction (XRD) using a D/Max-2400 diffractometer (Rigaku, Japan) at a scanning rate of 15° min^{-1} in the 2θ range from 20 to 80°, with C_uK_α radiation (= 1.5406 Å) at 40 kV and 100 mA. Optical absorption spectra of TiO_2 film and TiO_2/CdS_xSe_{1-x} photoanodes were recorded with a Jasco-V570 UV−Vis−NIR spectrophotometer equipped with an integrating sphere. Current density−voltage ($J-V$) measurement was performed with a Keithley 2400 source meter under one sun irradiation (AM 1.5 G, 100 mW cm^{-2}) from a solar simulator (Sciencetech Inc., SS-150). The incident photon-to-current conversion efficiency (IPCE) was measured as a function of wavelength from 300 to 800 nm by using a model 7-SCSpec II system (Beijing 7-Star Optical Instruments Co., Ltd.). For the open-circuit voltage-decay (OCVD) measurements, the cells were illuminated to a steady voltage (V_{OC}) with simulated AM 1.5 G at 100 mW cm-2, then the illumination was switched off, and the transient V_{OC} was recorded every 50 ms with the CHI 660D electrochemical workstation.

3. RESULTS AND DISCUSSION

This in situ hydrothermal method integrates linker assisted adsorption and colloidal quantum dot synthesis in a single step

due to the use of bifunctional molecular linkers (TGA), which have been widely used to tether organic-based QDs to oxides.[35,36] TiO_2 has a strong affinity for the carboxylate group of the linker molecules, as demonstrated previously with a variety of sensitizing dyes.[37,38] Thiol groups, on the other hand, bind strongly to CdS_xSe_{1-x} QDs through surface Cd^{2+} cations.[39] The covalent connection will accelerate the photo-induced carrier separation in the QDs sensitizer and therefore leads to a photocurrent enhancement for solar cell. Through the immersion of the TiO_2 films in the CdS_xSe_{1-x} QDs precursor solution for hydrothermal reaction, the QDs precursor will diffuse into the porous structure and bind chemically to the TiO_2 surfaces through the TGA linker (Figure 1), and the subsequent hydrothermal-treatment can

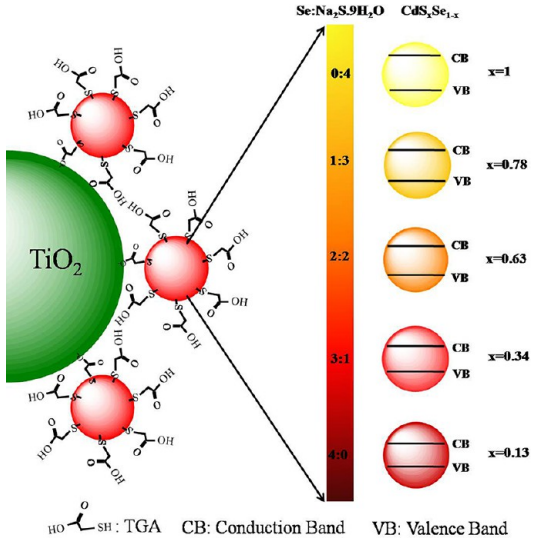

Figure 1. Schematic diagram depicting the band structure of various CdS_xSe_{1-x} QDs and the connection between TiO_2 and alloyed CdS_xSe_{1-x} QDs through linking molecules of TGA.

promote the growth and crystallization of CdS_xSe_{1-x} QDs. The ion-scale dimension of QDs precursor favors their easy diffusion within the porous structure and hence can access more surface of the TiO_2 than already-synthesized colloidal QDs. Therefore, this in situ hydrothermal method favors the formation of a well-covering QDs layer on mesoporous TiO_2 surface.

Figure 2 shows the surface morphologies of the bare mesoporous TiO_2 film and the TiO_2/CdS_xSe_{1-x} photoanodes prepared with $Se:Na_2S{\cdot}9H_2O$ = 0:4 and 2:2 feed molar ratios. As we can see, the bare film exhibits highly porous nanostructures of TiO_2 nanoparticles with an average size of 25 nm (Figure 2a), and the pore diameter of the screen-printed TiO_2 is in the range of 30−70 nm. This porous structure favors an easy penetration of electrolyte, as well as CdS_xSe_{1-x} precursors, during hydrothermal reaction process. After hydrothermal treatment in different CdS_xSe_{1-x} precursors at 160 °C for 12 h, the mesoporous structure of TiO_2 is still retained, which implies that the polysulfide electrolyte can well penetrates the photoanode for solar cell applications. However, the pore size of the TiO_2 becomes smaller, as shown in images b and c Figure 2, and the surface of TiO_2 particles becomes coarser after hydrothermal treatment, and the pore size of the TiO_2 decreased to 10−40 nm, and some pores were even clogged, which indicates a successful deposition of CdS_xSe_{1-x} QDs on the surface of the TiO_2 film.

To further confirm the formation of CdS_xSe_{1-x} QDs, we analyzed the bare TiO_2 film and TiO_2/CdS_xSe_{1-x} photoanodes by EDX spectra. Figure 2d−f shows the EDX dot scanning spectrum of the center scope within the bare TiO_2 (Figure 2d) and TiO_2/CdS_xSe_{1-x} photoanode prepared with $Se:Na_2S{\cdot}9H_2O$ = 0:4 (Figure 2e) and 2:2 (Figure 2f). The characteristic peaks of Cd, Se, and/or S elements, which are not shown in the EDX analysis of the bare TiO_2 film, appear after hydrothermal treatment in different QDs precursors, indicating that CdS_xSe_{1-x} QDs have been successfully assembled onto the TiO_2 surface.

The uniform distribution of QDs along the TiO_2 thickness is verified by the elemental analysis performed on cross sections of the TiO_2/CdS_xSe_{1-x} photoanode using an energy dispersive spectrometer equipped on a scanning electron microscope. The typical FESEM image of the cross section of the photoanode prepared with $Se:Na_2S{\cdot}9H_2O$ = 4:0 is shown in Figure 3a. The thickness of TiO_2 film was measured to be 9.41 μm, and this result agrees well with the profilometer measurement result. The Cd/Ti atomic ratio along the cross section of TiO_2 film is illustrated in Figure 3b. A nearly constant Ti/Cd ratio of 0.18 throughout the entire TiO_2 cross-section indicates homogeneous coverage of QDs on the TiO_2 film. This chemical analysis provides proof for effective penetration and homogeneous deposition of the QDs throughout the mesoporous network down to the FTO substrate, reflecting the effectiveness of the in situ hydrothermal method in TiO_2 sensitization. The effective penetration of the CdS_xSe_{1-x} QDs across the TiO_2 film can also be observed through the naked eye, as there is no observable coloration difference between the front and back sides of the TiO_2/CdS_xSe_{1-x} photoanode as shown in the inset of Figure 3b.

Figure 4a provides the typical TEM image of the as-synthesized ternary CdS_xSe_{1-x} QDs prepared with $Se:Na_2S{\cdot}9H_2O$ = 4:0 feed molar ratio. Hydrothermally synthesized CdS_xSe_{1-x} QDs display a homogeneous size distribution with a mean particle size of about 3.9 nm. To observe morphology of the TiO_2/CdS_xSe_{1-x} photoanode in detail, we analyzed TEM image of CdS QDs-sensitized TiO_2 film ($Se:Na_2S{\cdot}9H_2O$ = 0:4). As shown in Figure 4b, many CdS QDs can be clearly observed, distributed randomly over the TiO_2 surface, which is supported by our observation in the FESEM images. Figure 4c shows a high-magnification TEM image of TiO_2/CdS_xSe_{1-x} photoanode prepared with $Se:Na_2S{\cdot}9H_2O$ = 0:4 feed molar ratio. The lattice spacing measured for the crystalline plane is 0.22 nm, corresponding to the (111) plane of rutile TiO_2 (JCPDS 16−0934). Around the TiO_2 crystallite edge, fine crystallites are observed. By careful measurement and comparison of the lattice parameters with the data in JCPD, the crystallites connecting to TiO_2 have a lattice fringe of 0.205 nm, which is ascribed to the (220) plane of CdS (JCPDS 10−0454).These results of the SEM, EDX and TEM characterization demonstrate that this hydrothermal method is an efficient TiO_2 sensitization strategy for obtaining well-covering QDs layer on the TiO_2 surface.

Figure 5a shows XRD patterns of the bare TiO_2 film and the TiO_2/CdS_xSe_{1-x} photoanodes prepared with $Se:Na_2S{\cdot}9H_2O$ = 0:4 and $Se:Na_2S{\cdot}9H_2O$ = 4:0 feed molar ratios. The curve for bare TiO_2 was measured from a sample of TiO_2 mesoporus film printed on a FTO glass substrate. Diffraction peak positions of TiO_2 and SnO_2 from the FTO substrate are marked

dx.doi.org/10.1021/am4009924 | ACS Appl. Mater. Interfaces 2013, 5, 5139−5148

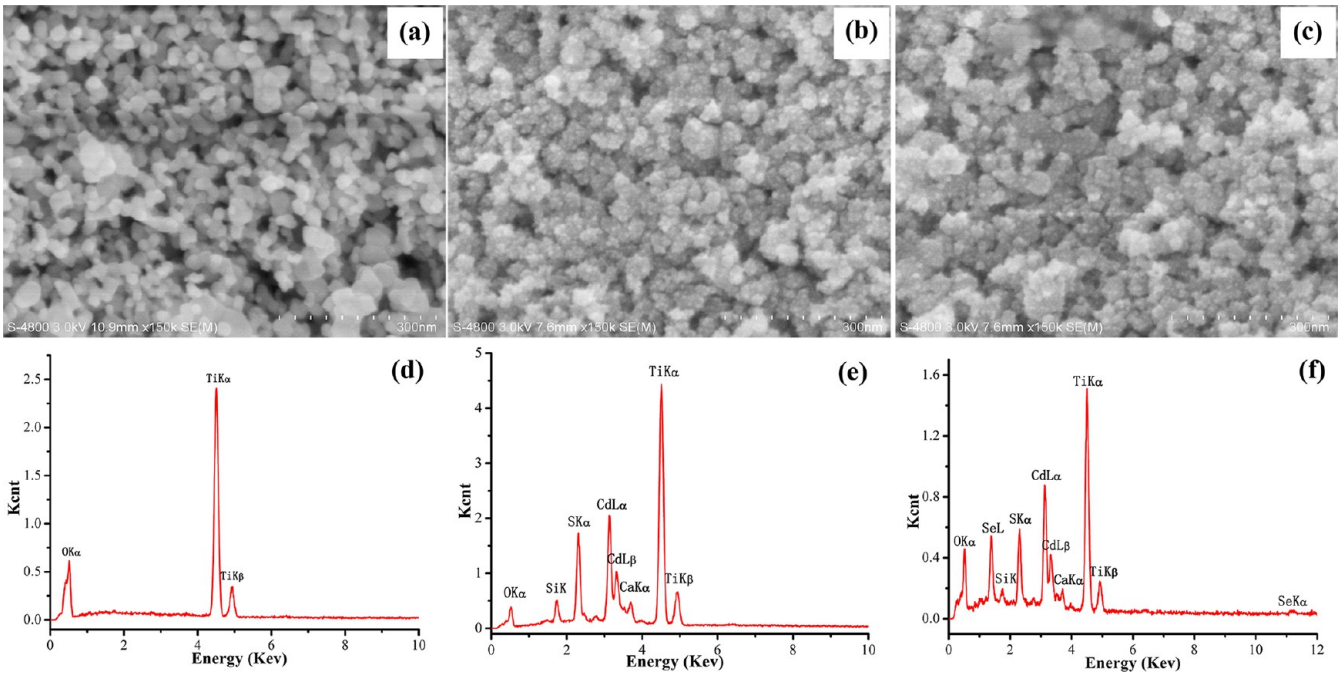

Figure 2. FESEM surface morphologies of (a) the bare mesoporous TiO_2 film, the TiO_2/CdS_xSe_{1-x} photoanodes prepared with (b) $Se:Na_2S{\cdot}9H_2O$ = 0:4 and (c) $Se:Na_2S{\cdot}9H_2O$ = 2:2 feed molar ratios, and (d–f) the corresponding EDX spectra, respectively.

respectively with filled and hollow circles. For bare TiO_2 film, the peaks at 25.3 and 27.5° are the characteristic reflection for anatase and rutile, respectively (JCPDS file No. 21−1272 and 21−1276). For TiO_2/CdS_xSe_{1-x} photoanodes prepared with $Se:Na_2S{\cdot}9H_2O$ = 0:4 and $Se:Na_2S{\cdot}9H_2O$ = 4:0, a new broad peak centered at 43.9° and 42.6° is observed, respectively. This broad peak can be assigned to the (220) plane of the cubic CdS_xSe_{1-x} alloyed QDs (JCPDS file No. 10−0454 and 19−0191). The XRD results confirm again the formation of CdS_xSe_{1-x} QDs on TiO_2 film.

Figure 5b depicts the powder XRD patterns of the TGA-capped CdS_xSe_{1-x} QDs prepared with different $Se:Na_2S{\cdot}9H_2O$ feed molar ratios, which were precipitated from aqueous solution with an excess of 2-propanol. For comparison, the standard XRD patterns of cubic CdSe and CdS were also shown. From the XRD patterns, it can be found that the synthesized CdS_xSe_{1-x} QDs have a cubic crystal structure, as indicated by the lack of diffraction peaks of (102) and (103) planes, which are characteristic of a hexagonal crystal structure.[40] Moreover, the diffraction peaks of the resulting alloyed QDs, which are positioned between that of the cubic CdS and CdSe phases, are gradually shift to lower angle with increasing Se feed amount. A dashed line has been included in Figure 5b to guide the eye. According to Bragg's law, such downshift of peak position indicates an increase in lattice parameter, and this agrees well with the difference in ionic radius between S^{2-} and Se^{2-}. The XRD results of CdS_xSe_{1-x} QDs suggest the formation of homogeneous alloy rather than a physical mixture of CdS and CdSe, which otherwise would have shown a superposition of the reflections from pure CdS and pure CdSe in the XRD.[31]

It is worth pointing out that the diffraction peaks of the CdS_xSe_{1-x} QDs prepared with $Se:Na_2S{\cdot}9H_2O$ = 4:0 feed molar ratio moved slightly toward higher angles compared with standard diffraction data of bulk CdSe with cubic structure. It indicates that there are some trace of CdS in the obtained CdSe QDs with $Se:Na_2S{\cdot}9H_2O$ = 4:0. This phenomenon is probably caused by the thermal decomposition of surface ligand (TGA) during hydrothermal process, which causes the incorporation of the sulfur element from the thiol group into the growing CdSe QD. This phenomenon has also been observed by A. L. Rogach and W. Yang et al.[41,42] The thermal decomposition of TGA results in the difference between the ratios of S/(S+Se) in the obtained ternary QDs and that in the precursor solution. To estimate the real composition of the alloyed CdS_xSe_{1-x} QDs, we used the Bragg's law and Vegard's law[43,44] to get the calculation values (approximate to real values) of the above five different samples, which are CdS_1Se_0, $CdS_{0.78}Se_{0.22}$, $CdS_{0.63}Se_{0.37}$, $CdS_{0.34}Se_{0.66}$, and $CdS_{0.13}Se_{0.87}$, corresponding to a feed molar ratio of $Se:Na_2S{\cdot}9H_2O$ = 0:4, 1: 3, 2:2, 3:1, and 4:0, respectively. Figure 6 shows the relative amount of sulfur in the product versus the relative amount of sulfur in the precursor solution. A deviation between the S/(S+Se) ratio in the precursor and the S/(S+Se) ratio incorporated into the alloyed CdS_xSe_{1-x} QDs was observed. For example, only 50% S in the precursor is needed to make alloyed CdS_xSe_{1-x} QDs with 63% S composition. More S element incorporated indicates that the TGA capping ligand also act as the source of sulfur, supplying sulfur monomers to construct the alloyed CdS_xSe_{1-x} QDs.

The broad diffraction peaks in Figure 5b imply that the CdS_xSe_{1-x} QDs are very small, and the average size of the QDs in each case can be calculated from the full-width at half-maximum (fwhm) of the (111) zinc blend reflection according to the Scherrer's formula. The sizes estimated for the CdS_xSe_{1-x} QDs prepared with $Se:Na_2S{\cdot}9H_2O$ precursor ratios of 0:4, 1:3, 2:2, 3:1, and 4:0 are 3.04, 3.12, 3.24, 3.46, and 3.65 nm, respectively, indicating slight increase in size with an increase in the Se feed amount. Such a relationship is consistent with the fact that the bond length of Cd−Se is larger than that of Cd−S. Obviously, the QDs size estimated from HRTEM is larger than that estimated from the XRD patterns. This difference is

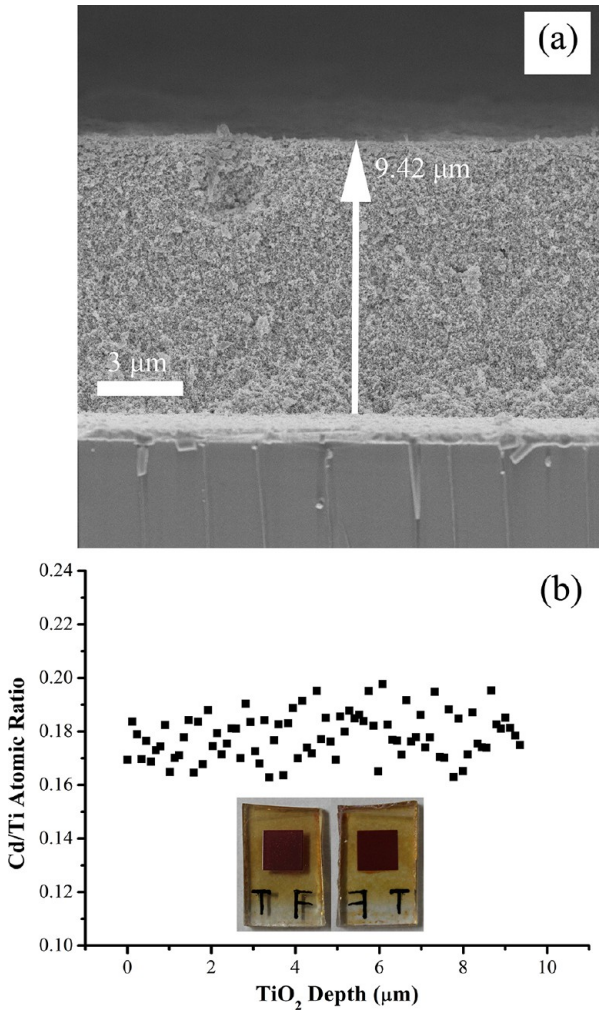

Figure 3. (a) FESEM image of a cross-section of TiO_2/CdS_xSe_{1-x} photoanode prepared with $Se:Na_2S{\cdot}9H_2O$ = 4:0 feed molar ratio, (b) Cd/Ti ratio along the cross section of TiO_2 film. The inset of panel b shows digital images of the front and back side of this TiO_2/CdS_xSe_{1-x} photoanode.

common in the case of QDs. It is worth noting that the Scherrer's formula estimates the size of single-crystalline domains (having periodic lattice) but not the actual size of the QDs. Therefore, it is expected that the QD size obtained from XRD patterns is always smaller than that estimated from HRTEM images.[45]

Optical pictures of bare TiO_2 film and five representative TiO_2/CdS_xSe_{1-x} photoanodes with different $Se/Na_2S{\cdot}9H_2O$ feed molar ratios are shown in Figure 7a. Visibly, these samples show single and unique colors with good uniformity across the substrate, and the color changes homogeneously from yellow to red as the $Se/Na_2S{\cdot}9H_2O$ ratio increased, which indicates an increase of CdSe content in alloyed QDs. Figure 7b shows the UV−visible absorption spectra of the bare TiO_2 film and as-prepared TiO_2/CdS_xSe_{1-x} photoanodes with various $Se/Na_2S{\cdot}9H_2O$ feed mole ratios. It can be seen that all samples exhibit a steep absorption edge in their respective spectra. Relative to the absorption edge of the bare TiO_2 film near 400 nm, the optical absorption of the TiO_2/CdS_xSe_{1-x} photoanodes can be tuned to cover a wide range of the visible spectrum. Arising from the smaller band gap of CdSe relative to CdS for a given size, we notice the red shift of the absorption edge of

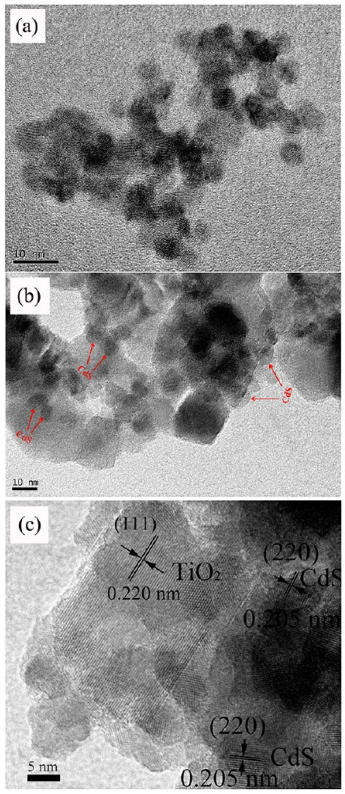

Figure 4. (a) High-magnification TEM image of CdS_xSe_{1-x} QDs prepared with $Se:Na_2S{\cdot}9H_2O$ = 4:0 feed molar ratio; (b) low-magnification and (c) high-magnification TEM images of TiO_2/CdS_xSe_{1-x} photoanode prepared with $Se:Na_2S{\cdot}9H_2O$ = 0:4 feed molar ratio.

TiO_2/CdS_xSe_{1-x} photoanodes with the increasing of Se composition, and this demonstrates that band gap tuning stems from stoichiometry variation in the ternary alloy CdS_xSe_{1-x} QDs. Such a continuous shift of the absorption edge of the TiO_2/CdS_xSe_{1-x} photoanodes with respect to their composition corroborate the observation of the well-crystallization of alloyed CdS_xSe_{1-x} QDs via intermixing of CdS and CdSe, rather than the formation of independent CdS and CdSe QDs.

Figure 8 shows a plot of band gaps of CdS_xSe_{1-x} alloys, calculated from the intersection points of the saturation line and incline lines of absorption spectrum as shown in Figure 7b (marked in violet), vs the composition ratios. The optical band gap is observed to vary nonlinearly with change in composition. The nonlinear dependence of band gap on composition can be attributed mainly to three factors, (i) the band structure may get altered with changing lattice constants, (ii) the redistribution of electrons because of the difference of electronegativity between the constituents compounds, and (iii) anion−cation bond lengths and angles must relax to accommodate the differently sized constituents.[32,46,47] As reported, the variation in the band gap of alloys with composition can be fitted by a quadratic function. In case of CdS_xSe_{1-x} alloy QDs, it is given by following equation[31,48]

$$E_g(x) = xE_{CdS} + (1-x)E_{CdSe} - bx(1-x) \quad (1)$$

where E_{CdS} and E_{CdSe} are the band gaps of the pure compounds CdS and CdSe, $E_g(x)$ is the band gap of the alloyed CdS_xSe_{1-x} QDs, and b is the optical bowing coefficient (bowing

dx.doi.org/10.1021/am4009924 | ACS Appl. Mater. Interfaces 2013, 5, 5139−5148

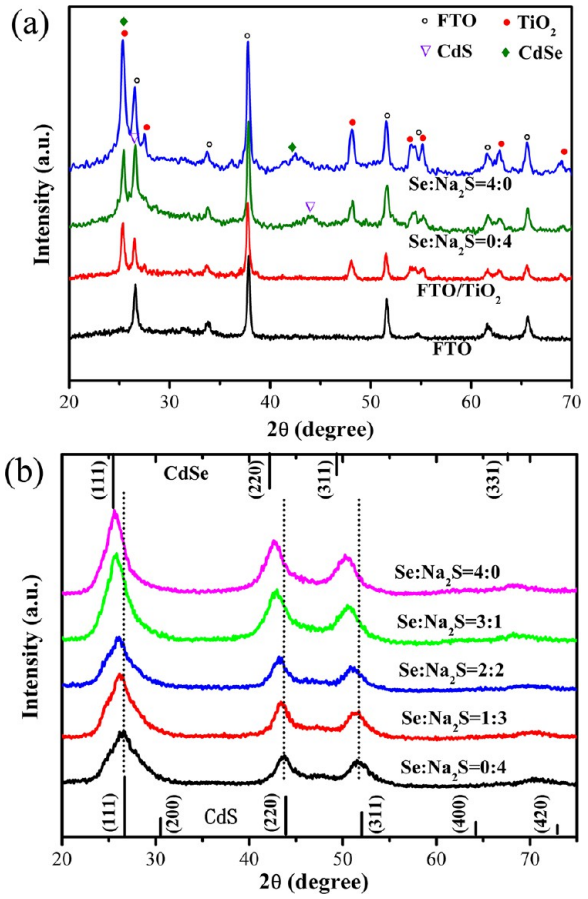

Figure 5. The XRD patterns of FTO, bare TiO_2 film and TiO_2/$CdSe_xS_{1-x}$ photoanode prepared with (a) $Se:Na_2S{\cdot}9H_2O$ = 0:4 and $Se:Na_2S{\cdot}9H_2O$ = 4:0 and (b) CdS_xSe_{1-x} QDs for different Se to $Na_2S{\cdot}9H_2O$ ratios. The standard patterns of bulk cubic CdSe and CdS in Figure 5b are present as references.

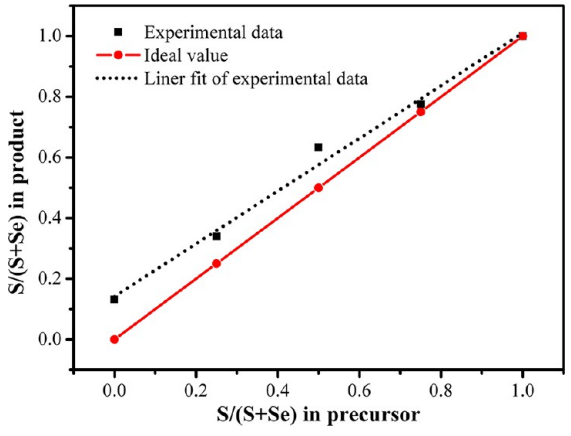

Figure 6. Relation of the relative amount of sulfur in the alloyed CdS_xSe_{1-x} QDs versus the relative amount of sulfur in the precursor solution determined from XRD patterns of CdS_xSe_{1-x} QDs.

parameter) that describes the extent of nonlinearity. For the determination of bowing constant b, the data of band gap as a function of composition for CdS_xSe_{1-x} QDs obtained from the present study were fitted into eq 1. Based on the fitting parameters, the bowing constant was estimated to be ca. 0.56 ± 0.12. This value of bowing constant is very close to that reported by Hill et al.[49,50] The relatively small value of b indicates that the synthesized CdS_xSe_{1-x} alloy QDs have good miscibility.

The results of UV−vis absorption and XRD demonstrate that the composition (Se vs S) of the resulting CdS_xSe_{1-x} QDs, from our batches with the different $Se/Na_2S{\cdot}9H_2O$ feed molar ratios, plays a relatively important role in the band gap, as compared to their size. For example, CdS_1Se_0 QDs exhibit absorption edge positioning at ∼506 nm with a size of ∼3.04 nm, whereas $CdS_{0.13}Se_{0.87}$ positions at 662 nm with a size of ∼3.65 nm. It is clear that the size variation is relatively small, but the composition and band gap variation is relatively large. Therefore, by varying the composition of the QDs, we have introduced an additional means of tuning their optical properties.

Figure 7c shows the absorption spectrum of TGA-capped CdS_xSe_{1-x} QDs with different $Se/Na_2S{\cdot}9H_2O$ ratios. Their absorption edges exhibit a red-shift from 480 nm through 518, 562, and 610 to 641 nm with increasing Se content in the ternary CdS_xSe_{1-x} QDs. It is noteworthy that the absorption edges of the TiO_2/CdS_xSe_{1-x} photoanodes shows a red shift of more than 15 nm as compared to the absorption edges of solution-grown CdS_xSe_{1-x} QDs with various $Se/Na_2S{\cdot}9H_2O$ ratios. This may be due to the fact that the TGA-capped QDs aggregated to some degree in the confined pores of TiO_2 during the hydrothermal reaction process.

To investigate the photovoltaic performance of the various TiO_2/CdS_xSe_{1-x} photoanodes, sandwich-type thin layer cells were fabricated with platinized ITO as the cathode, and a polysulfide electrolyte as the hole transporter. The $J-V$ curves corresponding to cell devices sensitized by different CdS_xSe_{1-x} QDs under the illumination of a solar simulator (AM 1.5 G) at 100 mW cm^{-2} are shown in Figure 9a, and the photovoltaic parameters including short circuit current density (J_{sc}), open circuit voltage (V_{oc}), fill factor (FF), and power conversion efficiency (η) are summarized in Table 1. For the built cell devices, the photovoltaic parameters show a clear dependence on composition of the CdS_xSe_{1-x} QDs sensitizer. The cell based on the photoanode prepared with $Se:Na_2S{\cdot}9H_2O$ = 0:4 gives a J_{sc} of 2.17 mA cm^{-2}, a V_{oc} of 0.55 V, and a FF of 0.31, yielding a power conversion efficiency of 0.37%. With an increase in $Se:Na_2S{\cdot}9H_2O$ molar ratio, the J_{sc} and V_{oc} increase to 8.72 mA cm^{-2} and 0.65 V for $Se:Na_2S{\cdot}9H_2O$ = 4:0. Thus the resulting η increases to 2.23%. The increased J_{sc} is mainly due to the expanded absorption spectrum coverage of the TiO_2/CdS_xSe_{1-x} photoanodes with more Se content. The J_{sc} is dependent on the combination of light harvesting efficiency (η_{lh}), charge injection efficiency (η_{inj}), and charge collection efficiency (η_{cc}). The higher η_{lh} will generate more photoexcited electrons, thus giving higher J_{sc}. Accordingly, the V_{oc} is also slightly enhanced following the trend of J_{sc}, possibly because of an increase in the amount of the electrons transported from the CdS_xSe_{1-x} QDs into the TiO_2 conduction band, leading to the increase in the quasi-Fermi level of TiO_2.[51] Previous studies have revealed that the mechanism behind the electron transfer at QD−molecule−substrate interfaces is quantum tunneling.[52−54] In this model, the electron transfer rate is expected to vary exponentially with the tunneling distance, the length of which in CdSe−linker−TiO_2 systems corresponds directly with the linker (TGA) length. In this regard, in comparison with mercaptopropanoic acid (MPA) or cysteine (Cys), the use of the short-chain TGA molecular would enhance the electronic coupling, and consequently facilitate electron injection, between QD and TiO_2 substrate. The improved fill factor of

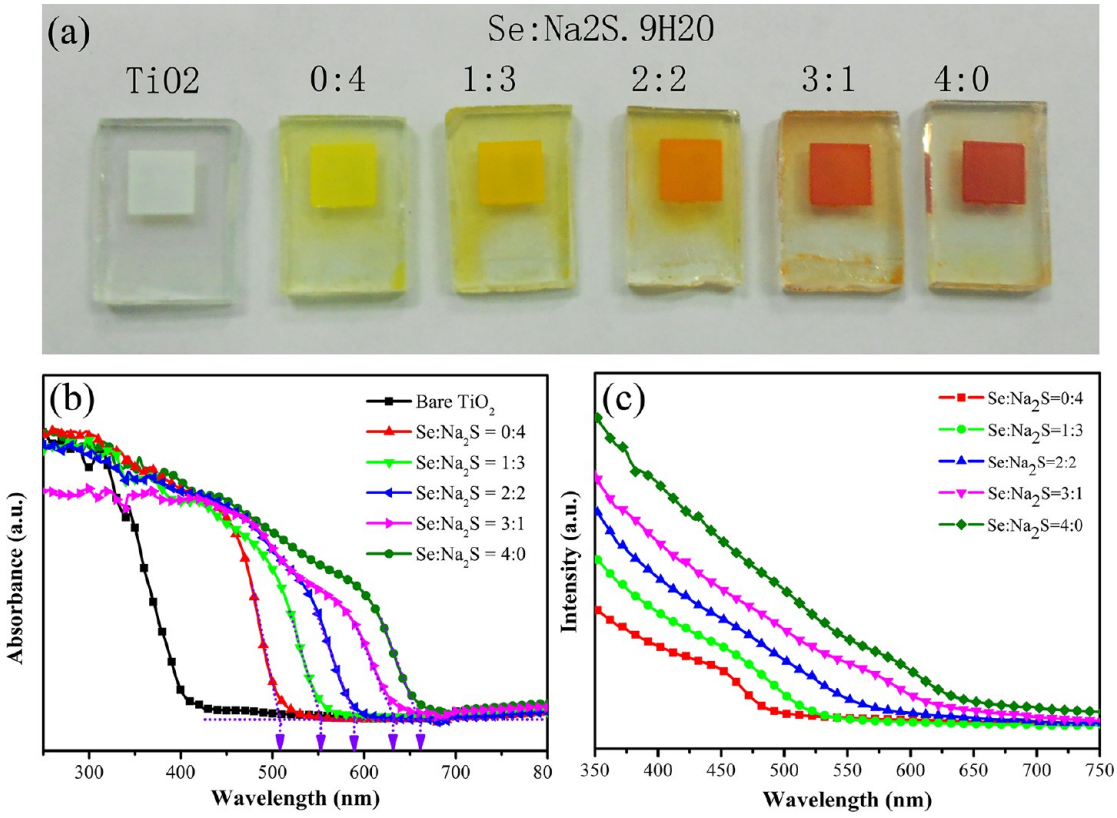

Figure 7. (a) Photographs and (b) UV–vis absorption spectra of bare TiO_2 film and TiO_2/CdS_xSe_{1-x} photoanodes prepared with different Se/$Na_2S{\cdot}9H_2O$ feed molar ratios.

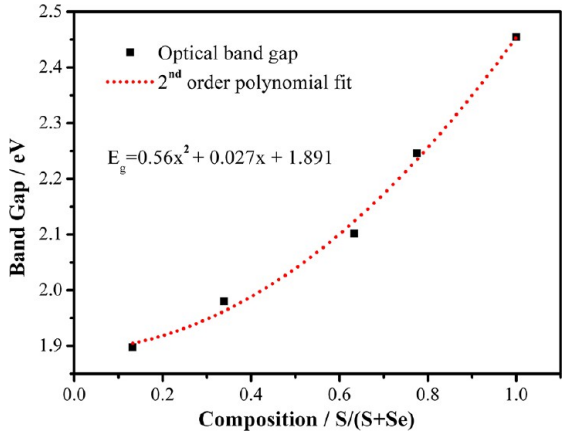

Figure 8. Plot of optical band gap of CdS_xSe_{1-x} alloy QDs as a function of sulfur mole fraction. The dash line indicates the second order polynomial to the experimental data.

the solar cell prepared with Se:$Na_2S{\cdot}9H_2O$ = 4:0 compared with that of the cell prepared with Se:$Na_2S{\cdot}9H_2O$ = 0:4 is probably due to the smaller series resistance (R_s), which can be expressed as

$$R_s = R_{TCO} + R_{ct} + R_{diff} \quad (2)$$

where R_{TCO} and R_{diff} are the substrate resistance and diffusion impedance in the electrolyte, respectively.[55,56] R_{ct} is the charge transfer resistance at the counter electrode–electrolyte interface. Because of the same conditions of device fabrication, the value of R_{TCO} and R_{diff} of these different solar cells can be considered the same. The value of R_{ct} is dependent on the redox reaction rate between QDs and the polysulfide electrolyte.[21] The $CdS_{0.13}Se_{0.87}$ QDs are able to generate more electron–hole pairs than CdS_1Se_0 QDs due to their broad absorption spectra, and the higher concentration of excited holes cause faster chemical reaction in the electrolyte, reducing the value of R_{ct}. The decrease in the R_{ct} with Se:$Na_2S{\cdot}9H_2O$ = 4:0 leads to a reduction in R_s and corresponding improvement in the FF.

The incident photon to charge carrier generation efficiency (*IPCE*) of the solar cell based on the TiO_2/CdS_xSe_{1-x} photoanode prepared with Se:Na2S·$9H_2O$ = 4:0 is shown in Figure 9b. It can be seen that the profile of IPCE plot corresponds well with the UV–visible absorption results, indicating that most of the absorbed light by QDs is involved in the photocurrent generation. The IPCE reaches a maximum of 46% at 495 nm and remains at a level over 40% up to 565 nm. This relatively good IPCE value indicates that this sensitization strategy holds great promise for the construction of high performance QDSSC.

Electron lifetimes of various alloyed CdS_xSe_{1-x} QDs-sensitized solar cell were estimated through open circuit voltage decay (OCVD) measurements.[51,57] Figure 10a shows V_{oc} decay curves of the QDSSCs recorded during relaxation from an illuminated quasi-equilibrium state to darkness. Clearly, after the light is switched off, there is still substantial concentration of charges (as evidenced e by the voltage) in the cells even after 80 s in the dark. This decay time is much larger than that of previously reported QDSSC prepared with the traditional successive ionic layer adsorption and reaction (SILAR) or chemical bath deposition (CBD) methods.[58–60] For example, the V_{oc} of those cells usually decay to 0.2 V in less than 20 s after the light is turned off, whereas it takes nearly 70

dx.doi.org/10.1021/am4009924 | ACS Appl. Mater. Interfaces 2013, 5, 5139–5148

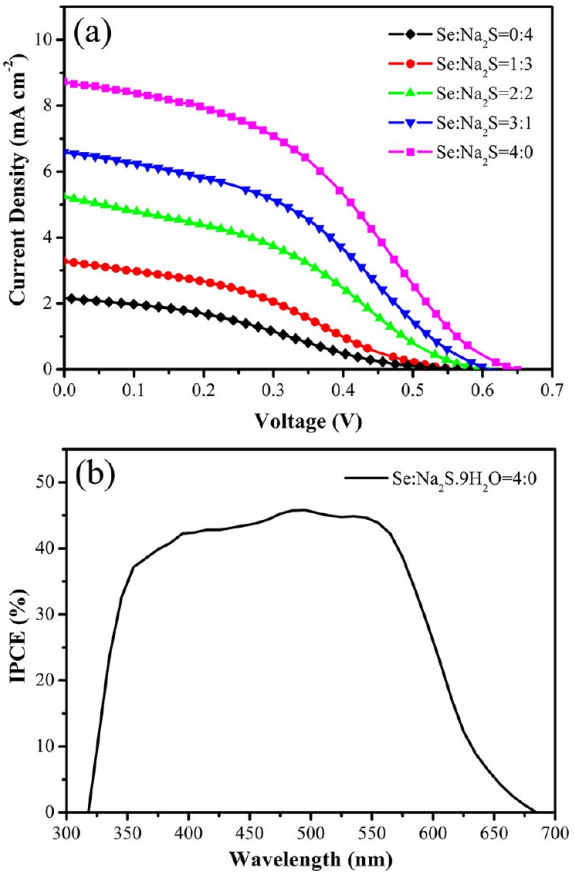

Figure 9. (a) Current density–voltage (J–V) characteristics of the QDSSC based on various TiO_2/CdS_xSe_{1-x} photoanodes, and (b) IPCE spectra of QDSSCs assembled with the TiO_2/CdS_xSe_{1-x} photoanode prepared with $Se:Na_2S{\cdot}9H_2O$ = 4:0.

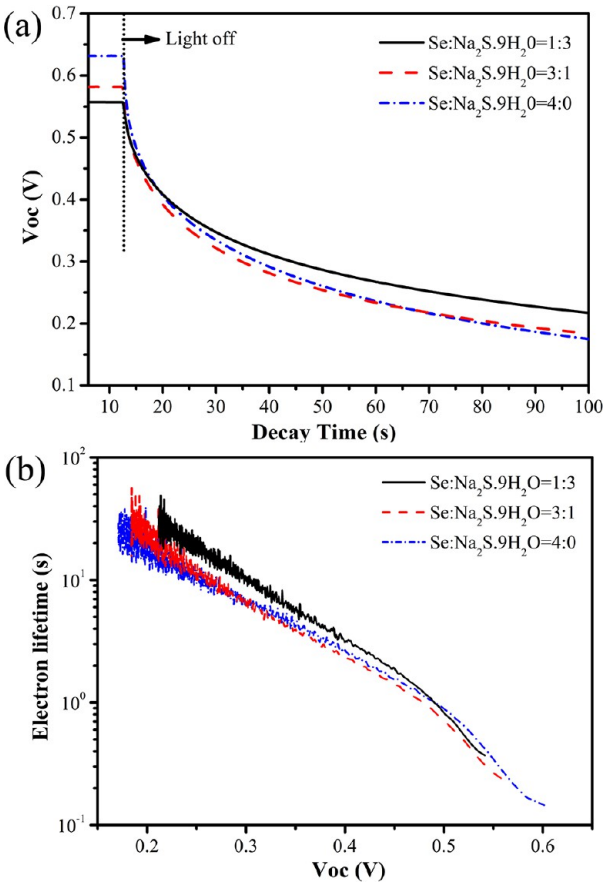

Figure 10. (a) V_{oc} decay curves of the QDSSCs prepared with $Se:Na_2S{\cdot}9H_2O$ = 0:4, 1:3, and 3:1 recorded during the relaxation from illuminated quasi-equilibrium to the dark. (b) Lifetime of electrons obtained from V_{oc} decay measurements.

Table 1. Photovoltaic Parameters Obtained from the J–V Curves of QDSSCs Using Various TiO_2/CdS_xSe_{1-x} Photoanodes

photoanodes	V_{oc} (V)	J_{sc} (mA cm^{-2})	FF (%)	η (%)
$Se:Na_2S$ = 0:4	0.55	2.17	31.02	0.37
$Se:Na_2S$ = 1:3	0.55	3.28	34.92	0.63
$Se:Na_2S$ = 2:2	0.56	5.25	38.78	1.14
$Se:Na_2S$ = 3:1	0.61	6.36	39.69	1.54
$Se:Na_2S$ = 4:0	0.65	8.72	39.34	2.23

s for our cell. The V_{oc} decay rate is directly related to electron lifetime, because excess electrons are removed through recombination when the illumination of the QDSSC at open circuit is interrupted. The effective electron lifetime, τ_e, of the QDSSCs at different voltage can therefore be estimated from the V_{oc} decay curves according to eq 3.[51,57]

$$\tau_e = -\frac{k_{BT}}{e}\left[\frac{dV_{oc}}{dt}\right]^{-1} \quad (3)$$

where k_{BT} is the thermal energy and e is the positive elementary charge. Figure 10b illustrates the τ_e of the QDSSC prepared with $Se:Na_2S{\cdot}9H_2O$ = 0:4, 1:3, and 3:1 as a function of voltage. The electron lifetime of all the cells increases with the decreasing V_{oc} but changes little with alloy composition. The lifetime spans 2 orders of magnitude, from 0.3 to 30 s. In comparison to reported OCVD measurements of QDSSC prepared with SILAR or CBD methods,[58−60] the solar cells in the present study exhibit superior recombination characteristics, with the longer lifetimes indicating fewer recombination. M. Miyauchi's group reported that the charge recombination from the TiO_2 to the electrolyte is mainly responsible for the V_{oc} decay of the QDSSCs.[59] The slower V_{oc} decay and longer electron lifetime of the QDSSC presented in this study indicate that this hydrothermal method effectively suppresses the electron back transfer process from TiO_2 to electrolyte because of the well-covered QDs layer on the TiO_2 surface.

The photostability of photochemical solar cell is another very important issue. Thus we have investigated the stability of this CdS_xSe_{1-x} QDs-sensitized solar cell by measuring J_{sc} with respect to time under the continuous illumination (Figure 11). During the first 1 h of illumination, a stable photocurrent density of 8.7 mA cm^{-2} was observed, which indicates a good stability of the device during the measurement. The photostability could be attributed to efficient hole scavenging capability of polysulfide electrolyte, which successfully suppresses hole-induced anodic corrosion of the CdS_xSe_{1-x} QDs.

Despite an acceptable efficiency of 2.23% has been achieved by using this CdS_xSe_{1-x} alloy QDs as sensitizer, we believe that there is still much room for further very substantial improvement of the power conversion efficiency, in particular by augmentation of the J_{sc} and FF through further reduction of the series resistance of cells. For example, a ZnS capping layer and annealing treatment may reduce the undesired surface trapping

dx.doi.org/10.1021/am4009924 | ACS Appl. Mater. Interfaces 2013, 5, 5139−5148

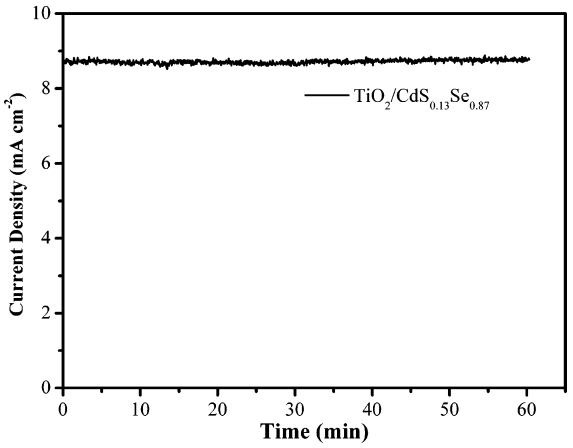

Figure 11. Photocurrent stability of CdS_xSe_{1-x} QDs-sensitized solar cell under continuous illumination of 100 mW cm^{-2}.

processes and enhance the photogenerated electrons transfer from excited CdS_xSe_{1-x} QDs to TiO_2, thereby leading to an improved performance in QDSSCs. This will be the focus of our continuing investigations. This in situ hydrothermal method, together with the use of alloyed QDs as sensitizer, opens up new avenues for future development of high-efficiency QDSSC.

4. CONCLUSIONS

In summary, composition-tunable alloyed CdS_xSe_{1-x} QDs is successfully synthesized directly in aqueous solution and simultaneously in situ deposited on mesoporous TiO_2 films. This hydrothermal technique achieves high coverage and uniform distribution of CdS_xSe_{1-x} QDs within TiO_2 films. By tuning the precursor ($Se/Na_2S{\cdot}9H_2O$) ratio, the optical band gap and consequently the band energies of the resulting CdS_xSe_{1-x} QDs can feasibly be adjusted between the energy levels of CdSe and CdS QDs of similar dimensions. The suitable Se content (x = 0.13) in CdS_xSe_{1-x} QDs strike a balance between a broad optical absorption and a suitable energy band alignment. In comparison with binary QDs, this ternary alloyed QDs sensitizer provides an additional degree of freedom in selecting desirable properties for QDSSC because their physical and optical properties depend on both size and composition. Based on these $CdSe_xS_{1-x}$ QDs sensitized mesoporous TiO_2 photoanodes, the assembled QDSSC yield a maximum power conversion efficiency of 2.23% under AM 1.5 illumination of 100 mW cm^{-2}. The flexibility of tailoring optical properties of semiconductor sensitizer makes this composition tuned approach a very promising synthetic method for preparation of highly efficient photoanodes for QDSSC.

■ ASSOCIATED CONTENT

Supporting Information

This material is available free of charge via the Internet at http://pubs.acs.org.

■ AUTHOR INFORMATION

Corresponding Author

*E-mail: mqwang@mail.xjtu.edu.cn. Tel. & fax: +86 29 82668794.

Notes

The authors declare no competing financial interest.

■ ACKNOWLEDGMENTS

The authors gratefully acknowledge financial support from Natural Science Foundation of China (Grants 61176056 and 91123019). This work has been financially supported by the International Collaboration Program and the "13115" Innovation Engineering Project of Shaanxi Province (Grants 2013KW-12-05 and 2010ZDKG-58) and by the open projects from Institute of Photonics and Photo-Technology, Provincial Key Laboratory of Photoelectronic Technology, Northwest University, China.

■ REFERENCES

(1) Moreels, I.; Justo, Y.; Geyter, B. D.; Haustraete, K.; Martins, J. C.; Hens, Z. *ACS Nano* **2011**, *5*, 2004−2012.
(2) Lin, Z.; Wang, M.; Zhang, L.; Xue, Y.; Yao, X.; Cheng, H.; Bai, J. *J. Mater. Chem.* **2012**, *22*, 9082−9085.
(3) Yu, W. W.; Qu, L.; Guo, W.; Peng, X. *Chem. Mater.* **2003**, *15*, 2854−2860.
(4) Alivisatos, A. P. *Science* **1996**, *271*, 933−937.
(5) Yang, Z.; Wang, M.; Shi, Y.; Song, X.; Lin, Z.; Ren, Z.; Bai, J. *J. Mater. Chem.* **2012**, *22*, 21009−21016.
(6) Nozik, A. J. *Physica E* **2002**, *14*, 115−120.
(7) Sambur, J. B.; Novet, T.; Parkinson, B. A. *Science* **2010**, *330*, 63−66.
(8) Semonin, O. E.; Luther, J. M.; Choi, S.; Chen, H.-Y.; Gao, J.; Nozik, A. J.; Beard, M. C. *Science* **2011**, *334*, 1530−1533.
(9) Zhu, G.; Pan, L.; Xu, T.; Sun, Z. *ACS Appl. Mater. Interfaces* **2011**, *3*, 1472−1478.
(10) Shen, Y.-J.; Lee, Y.-L. *Nanotechnology* **2008**, *19*, 045602.
(11) Kim, H; Jeong, H ; An, T. K.; Park, C. E. ; Yong , K. *ACS Appl. Mater. Interfaces* **2013**, *5*, 268−275.
(12) Hossain, M. A; Koh, Z. Y.; Wang, Q. *Phys. Chem. Chem. Phys.* **2012**, *14*, 7367−7374.
(13) Hossain, M. A; Jennings, J. R.; Koh, Z. Y.; Wang, Q. *ACS Nano* **2011**, *5*, 3172−3181.
(14) Lee, H. J.; Wang, M.; Chen, P.; Gamelin, D. R.; Zakeeruddin, S. M.; Grätzel, M.; Nazeeruddin, M. K. *Nano Lett.* **2009**, *9*, 4221−4227.
(15) Zhang, H.; Cheng, K.; Hou, Y. M.; Fang, Z.; Pan, Z. X.; Wu, W. J.; Hua, J. L.; Zhong, X. H. *Chem. Commun.* **2012**, *48*, 11235−11237.
(16) Im, S. H.; Kim, H.-J.; Kim, S. W.; Kim, S.-W.; Seok, S., II. *Energy Environ. Sci* **2011**, *4*, 4181−4186.
(17) Hossain, M. A.; Jennings, J. R.; Mathews, N.; Wang, Q. *Phys. Chem. Chem. Phys.* **2012**, *14*, 7154−7161.
(18) Zhang, Q.; Chen, G.; Yang, Y.; Shen, X.; Zhang, Y.; Li, C.; Yu, R.; Luo, Y.; Li, D.; Meng, Q. *Phys. Chem. Chem. Phys.* **2012**, *14*, 6479−6486.
(19) Santra, P. K.; Kamat, P. V. *J. Am. Chem. Soc.* **2012**, *134*, 2508−2511.
(20) Im, J.-H.; Lee, C.-R.; Lee, J.-W.; Park, S.-W.; Park, N.-G. *Nanoscale* **2011**, *3*, 4088−4093.
(21) Chen, Z.; Peng, W.; Zhang, K.; Zhang, J.; Yanagida, M.; Han, L. *Nanoscale* **2012**, *4*, 7690−7697.
(22) Baskoutas, S.; Terzis, A. F. *J. Appl. Phys.* **2006**, *99*, 013708.
(23) Aboulaich, A.; Billaud, D.; Abyan, M.; Balan, L.; Gaumet, J.; Medjadhi, G.; Ghanbaja, J.; Schneider, R. *ACS Appl. Mater. Interfaces* **2012**, *4*, 2561−2569.
(24) Kongkanand, A.; Tvrdy, K.; Takechi, K.; Kuno, M.; Kamat, P. V. *J. Am. Chem. Soc.* **2008**, *130*, 4007−4015.
(25) Mahmoud, W. E.; Al-Amri, A. M.; Yaghmour, S. J. *Opt. Mater.* **2012**, *34*, 1082−1086.
(26) Ma, W.; Luther, J. M.; Zheng, H.; Wu, Y.; Alivisatos, A. P. *Nano Lett.* **2009**, *9*, 1699−1703.
(27) Regulacio, M. D; Han, M.-Y. *Acc. Chem. Res.* **2010**, *43*, 621−630.
(28) Luther, J. M.; Law, M.; Beard, M. C.; Song, Q.; Reese, M. O.; Ellingson, R. J.; Nozik, A. J. *Nano Lett.* **2008**, *8*, 3488−3492.
(29) Rama Krishna, M. V.; Friesner, R. A. *J. Chem. Phys.* **1991**, *95*, 8309−8322.

(30) Wang, B.; Jiang, Y.; Liu, C.; Lan, X.; Liu, X.; Wang, W.; Duan, H.; Zhang, Y.; Li, S.; Zhang, Z. *Phys. Status Solidi A* **2012**, *209*, 306−312.
(31) Swaord, L. A.; Weigand, L. A.; Bowers, M. J., II; McBride, J. R.; Rapaport, J. L.; Watt, T. L.; Dixit, S. K.; Feldman, L. C.; Rosenthal, S. J. *J. Am. Chem. Soc.* **2006**, *128*, 12299−12306.
(32) Jang, E.; Jun, S.; Pu, L. *Chem. Commun.* **2003**, 2964−2965.
(33) Sung, T. K.; Kang, J. H.; Jang, D. M.; Myung, Y.; Jung, G. B.; Kim, H. S.; Jung, C. S.; Cho, Y. J.; Park, J.; Lee, C.-L. *J. Mater. Chem.* **2011**, *21*, 4553−4561.
(34) Kang, J. H.; Myung, Y.; Choi, J. W.; Jang, D. M.; Lee, C. W.; Park, J.; Cha, E. H. *J. Mater. Chem.* **2012**, *22*, 8413−8419.
(35) Mora-Seró, I.; Giménez, S.; Moehl, T.; Fabregat-Santiago, F.; Lana-Villareal, T.; Gómez, R.; Bisquert, J. *Nanotechnology* **2008**, *19*, 424007.
(36) Song, X.; Wang, M.; Shi, Y.; Deng, J.; Yang, Z.; Yao, X. *Electrochim. Acta* **2012**, *81*, 260−267.
(37) Nazeeruddin, M. K.; Kay, A.; Rodicio, I.; Humpbry-Baker, R.; Müller, E.; Liska, P.; Vlachopoulos, N.; Grätzel, M. *J. Am. Chem. Soc.* **1993**, *115*, 6382−6390.
(38) Asbury, J. B.; Anderson, N. A.; Hao, E.; Ai, X.; Lian, T. *J. Phys. Chem. B* **2003**, *107*, 7376−7386.
(39) Robel, I.; Subramanian, V.; Kuno, M.; Kamat, P. V. *J. Am. Chem. Soc.* **2006**, *128*, 2385−2393.
(40) Ouyang, J.; Vincent, M.; Kingston, D.; Descours, P.; Boivineau, T.; Zaman, M. B.; Wu, X.; Yu, K. *J. Phys. Chem. C* **2009**, *113*, 5193−5200.
(41) Rogach, A. L.; Kornowski, A.; Gao, M.; Eychmuller, A.; Weller, H. *J. Phys. Chem. B* **1999**, *103*, 3065−3069.
(42) Mao, W.; Guo, J.; Yang, W.; Wang, C.; He, J.; Chen, J. *Nanotechnology* **2007**, *18*, 485611.
(43) Cole, H. *J. Appl. Crystallogr.* **1970**, *3*, 405−406.
(44) Denton, A. R.; Ashcroft, N. W. *Phys. Rev. A* **1991**, *43*, 3161−3164.
(45) Dabbousi, B. O.; Rodriguez-Viejo, J.; Mikulec, F. V.; Heine, J. R.; Mattoussi, H.; Ober, R.; Jensen, K. F.; Bawendi, M. G. *J. Phys. Chem. B* **1997**, *101*, 9463−9475.
(46) Bernard, J. E.; Zunger, A. *Phys. Rev. B* **1987**, *36*, 3199−3228.
(47) Wei, S.-H.; Zhang, S. B.; Zunger, A. *J. Appl. Phys.* **2000**, *87*, 1304−1311.
(48) Pan, J.; Utama, M. I. B.; Zhang, Q.; Liu, X.; Peng, B.; Wong, L. M.; Sum, T. C.; Wang, S.; Xiong, Q. *Adv. Mater.* **2012**, *24*, 4151−4156.
(49) Lu, J.; Sun, C.; Zheng, M.; Mathews, N.; Liu, H.; Chen, G. S.; Zhang, X.; Mhaisalkar, S. G.; Haur, S. C. *J. Phys. Chem. C* **2011**, *115*, 19538−19545.
(50) Hill, R. *J. Phys. C: Solid State Phys.* **1974**, *7*, 521−526.
(51) Zaban, A.; Greenshtein, M.; Bisquert, J. *ChemPhysChem* **2003**, *4*, 859−864.
(52) Dibbel, R. S.; Youker, D. G.; Watson, D. F. *J. Phys. Chem. C* **2009**, *113*, 18643−18651.
(53) Hyun, B.-R.; Bartnik, A. C.; Sun, L.; Hanrath, T.; Wise, F. W. *Nano Lett.* **2011**, *11*, 2126−2132.
(54) Adams, D. M.; Brus, L.; Chidsey, C. E. D.; Creager, S.; Creutz, C.; Kagan, C. R.; Kamat, P. V.; Lieberman, M.; Lindsay, S.; Marcus, R. A.; Metzger, R. M.; Michel-Beyerle, M. E.; Miller, J. R.; Newton, M. D.; Rolison, D. R.; Sankey, O.; Schanze, K. S.; Yardle, J.; Zhu, X. *J. Phys. Chem. B* **2003**, *107*, 6668−6697.
(55) Hauch, A.; Georg, A. *Electrochim. Acta* **2001**, *46*, 3457−3466.
(56) Ramasamy, E.; Lee, W. J.; Lee, D. Y.; Song, J. S. *Electrochem. Commun.* **2008**, *10*, 1087−1089.
(57) Mor, G. K.; Shankar, K.; Paulose, M.; Varghese, O. K.; Grimes, C. A. *Nano Lett.* **2006**, *6*, 215−218.
(58) Kim, J.; Choi, H.; Nahm, C.; Kim, C.; Nam, S.; Kang, S.; Jung, D.-R.; Kim, J. I.; Kang, J.; Park, B. *J. Power Sources* **2012**, *220*, 108−113.
(59) Liu, Z.; Miyauchi, M.; Uemura, Y.; Cui, Y.; Hara, K.; Zhao, Z.; Sunahara, K.; Furube, A. *Appl. Phys. Lett.* **2010**, *96*, 233107.
(60) Jung, S. W.; Park, J.-H.; Lee, W.; Kim, J.-H.; Kim, H.; Choi, C.-J.; Ahn, K.-S. *J. Appl. Phys.* **2011**, *110*, 054301.